Multiphase flow of miscible liquids: jets and drops

Citation	Walker, T. W., Logia, A. N., & Fuller, G. G. (2015). Multiphase flow of miscible liquids: jets and drops. Experiments in Fluids, 56(5), 106. doi:10.1007/s00348-015-1974-y
DOI	10.1007/s00348-015-1974-y
Publisher	Springer
Version	Accepted Manuscript
Terms of Use	http://cdss.library.oregonstate.edu/sa-termsofuse

Experiments in Fluids manuscript No.
(will be inserted by the editor)

Multiphase flow of miscible liquids

Jets and drops

Travis W. Walker · Alison N. Logia · Gerald G. Fuller

Received: date / Accepted: date

Abstract Drops and jets of liquids that are miscible with the surrounding bulk liquid are present in many processes from cleaning surfaces with the aid of liquid soaps to the creation of biocompatible implants for drug delivery. Although the interactions of immiscible drops and jets show similarities to miscible systems, the small, transient interfacial tension associated with miscible systems create distinct outcomes such as intricate droplet shapes and breakup resistant jets.

Experiments have been conducted to understand several basic multiphase flow problems involving miscible liquids. Using high-speed imaging of the morphological evolution of the flows, we have been able to show that these processes are controlled by interfacial tensions. Further multiphase flows include investigating miscible jets, which allow the creation of fibers from inelastic materials that are otherwise difficult to process due to capillary breakup. This work shows that stabilization from the diminishing interfacial tensions of the miscible jets allow various elongated morphologies to be formed.

Keywords miscible · drops · transient interfacial tension

1 Introduction and Review

The interactions of jets and drops of liquids that are miscible with a surrounding, bulk liquid are central to numerous processes that range from cleansing operations where liquid soaps are rinsed from surfaces, to the dissolution of mucus in our intestinal tract. Although the dynamics of immiscible and miscible jets and drops bear some similarities, the very small and transient interfacial tensions, $\sigma(t)$, associated with miscible systems give rise to distinct outcomes such as droplets that have intricate shapes and jets that resist breakup. A useful review of these phenomena can be found in the book by Joseph and Renardy [21]. Importantly, when the unique structures derived from miscible, multicomponent flows are coupled with chemical reactions or phase transformations that can "freeze" in these morphologies, complex geometrical objects can be created from materials that are otherwise difficult to process.

1.1 Review of the impaction of drops into various media

The impaction of droplets into a deep liquid has been studied for over a century. Early work by Tomlinson [44] and later by Thomson and Newall [43] examined a variety of phenomena that occur when droplets of various materials fall into water, focusing on the now well-known formation of vortex rings. A few years later, Worthington began his study of splashing droplets by using short-exposure photography to resolve further details of the resulting morphology [48]. These works would become the foundation observations for droplet impaction, and to this day, they continue to be the majority of the work using different drop and bulk liquids.

The study of droplets impacting an interface can quickly become complicated with the numerous combinations of parameters that can be varied. Rein's 1993 review on liquid droplets impacting on solid and liquid interfaces provides a convenient survey of the parameters governing the impaction event [33]. The study describes coalescence and splashing on liquid surfaces, as well as cavitation and the entrain-

T.W. Walker
School of Chemical, Biological, and Environmental Engineering
Oregon State University
Corvallis, OR 97331, USA
E-mail: travis.walker@oregonstate.edu

A.N. Logia · G.G. Fuller
Department of Chemical Engineering
Stanford University
Stanford, CA 94305, USA

ment of gas. Rein goes on to mention that, when the droplet and the target liquid are different, further designation needs to be made between miscible and immiscible liquids. This designation will become the focus of this work.

1.1.1 Homogeneous drop impact

A number of works have been completed for the impaction of a droplet with a target liquid of the same material [2, 6, 7, 9–11, 14, 18, 19, 25, 28, 30–32, 34–36, 38, 39, 50]. The majority of the work has been focused on the entrainment of gas bubbles in the target liquid; however, some work has observed the transition from the various regimes that are present such as the transition from coalescence to splashing. This work has shown the complexity that exists when attempting to map the various regimes of a simple homogenous liquid drop impact into a deep pool.

1.1.2 Immiscible heterogeneous drop impact

Until recently, few studies have considered the impaction of droplets with an immiscible target liquid [5, 15, 46]. Fujimatsu et al. made detailed observations of the interfacial deformation of a water droplet impacting a silicone oil surface. Their work focused on the maximum depth of the cavity during impact and the maximum diameter of the water drop spreading on the oil surface, while documenting an interesting set of parameters that causes the droplet to be smashed into pieces.

1.1.3 Miscible heterogeneous drop impact

The interaction of a droplet with a miscible target liquid of a different material, studied mainly by the early investigators, has seen a resurgence in interest, driven by the goal of freezing the various morphologies seen during the impaction event. Deng et al. studied the prevention of bubble entrapment in a reactive heterogeneous system [12]. Their work focused on the surface quality of a polymer capsule formed during the impact of a viscous poly-anion drop into a poly-cation solution. They identified a specific regime in their Weber number versus Froude number phase space for their materials where bubble encapsulation was preventable. Even more recently, the Liu group [40, 41] studied the generation of "toroidal-spiral" particles by combining miscible drop impaction with polymerizable materials. This combination allowed them to "freeze" interesting morphologies that might find application as drug delivery vehicles. For this purpose, these authors developed a "phase diagram" in the impact Reynolds number, impact capillary number, impact Weber number, and drop/bulk viscosity ratio parameter space that specifies the operating conditions where impacting droplets penetrate and detach from the air/bulk interface to achieve distinct shapes. They focussed on toroidal shapes that folded to accommodate spiral, internal structures. By further controlling the Damköhler number (the ratio of reaction rate to convection rate) of a photo-initiated polymerization reaction, they were able to solidify the droplets and trap diffusible chemical species within high area-to-volume cavities.

A recent study by Hu et al. [20] looked at controlling microgel particles by combining microfluidics with an external ionic crosslinker. They were able to generate a number of varied shapes (e.g., mushroom-like, hemi-spherical, red blood cell-like) of alginate microgels by varying the gelation conditions such as the viscosity of the outer media and the interfacial tension.

1.2 Review of the translation of drops in miscible media

1.2.1 Translating miscible heterogeneous drops

One of the first studies of translating, miscible drops was reported by Kojima et al. [23]. That work focussed on the evolution of the shape of droplets of corn syrup-in-water descending through water, and experiments were conducted as the density and viscosity ratio of the drops and suspending fluids were varied. The drops were ejected through the air/bulk liquid interface after falling from variable heights above the bulk medium. The experiments were accompanied by theoretical predictions that considered two limiting cases: droplets that were only slightly deformed from sphericity and droplets in the shape of slender tori. The theory, while able to reproduce some of the qualitative nature of the limiting shape transitions, was unable to quantitatively reproduce aspects, such as the rate of torus expansion. Whereas the majority of predictions in that paper assumed the interfacial tension, σ, to be negligible, those authors concluded that this property must be present, although very small, at interfaces partitioning miscible liquids, while the system is not in equilibrium. The measurement of interfacial tension between miscible liquids is challenging not only because the values are small but also because they diminish in time as diffusion proceeds and the two liquids ultimately mix. In the absence of convection, the classic Cahn-Hilliard model [8] applied to a flat interface where the variable x measures depth, suggests that σ will vary with the concentration c of one component in a two-liquid system, as

$$\sigma(t) \approx \int \left[\frac{\partial c(x,t)}{\partial x} \right]^2 dx. \tag{1}$$

Since the evolution of $c(x,t)$ is expected to be controlled by diffusion, this approach leads to a prediction that, as time proceeds, the interfacial tension will decrease as $t^{-1/2}$.

Arecchi et al. [3] also examined translating, miscible drops and extended the experimental observations of Kojima et al. by reporting on a cascade of flow instabilities that include generation of expanding tori that fragment into arrays of smaller droplets. The sedimentation of miscible drops has also been studied within the confinement of a Hele Shaw cell by García et al. [16]. This work reported a similar cascade in the evolution of falling, miscible drops as found in three-dimensional space (passage to mushroom-shaped drops) with the exception that confinement suppressed the appearance of expanding tori.

1.2.2 Translating suspended particle drops

A body of work also exists reporting experiments and simulations on droplets of suspended particles descending through the suspending fluid. Powell and Mason [29] studied the deformation and breakup of cohesionless droplets of suspended particles experiencing either simple shear or pure elongation within a bulk consisting of the same suspending fluid. Qualitatively, the reported deformations of the particle clusters were similar in appearance to analogous experiments performed on suspended liquid droplets. Adachi et al. [1] examined the case of sedimenting particle clusters and accompanied their experiments with modeling efforts. They reported shape transitions in the clusters that bear remarkable similarity to those transitions described later by Kojima et al. for miscible, liquid drops. Schaflinger et al. [37] expanded on these observations and suggested that an interfacial tension exists between particle clusters and the bulk, suspending liquid. Schaflinger and co-workers [26] later followed with a very comprehensive study of sedimenting drops that included simulations that were able to achieve very nice correspondence with experiments. The observed phenomena included droplet deformation evolving towards tori that underwent instabilities towards cascades of daughter droplets.

1.3 Motivation

This work was initially motivated by the observation that viscous liquids, such as glycerol, that coat a surface will exhibit varying kinds of ablation when a jet of water is impinged normal to the surface. The variations include a possible undercutting phenomenon, where the water jet cuts under the viscous glycerol solution if the viscosity of the coating layer is below a certain value [45]. To focus on the initial interaction of the liquid jet with the bulk, we chose a well-controlled droplet and focused on the short-time impaction of the droplet. We soon realized that, when the impacting droplet of water is very small, the droplet will simply wet the surface of the viscous bulk. However, when the two fluids are interchanged so that a droplet of the highly viscous fluid impacts a bath of the less viscous fluid, a wide variety of beautiful morphological events arise that are often only appreciated when using a high-speed camera. These experiments are in the spirit of Tomlinson [44] and of Thomson [43], while also being similar to Taylor's experiments [42] of a viscous jet impacting a less viscous bulk. When viewing the raw videos in slow motion of glycerol impacting water, the effect of having two miscible fluids interacting with an interfacial tension that is small and decaying provides a variety of possibilities that would not be readily accessible if the two fluids were immiscible.

A major aim of this work was to explore an *expanded* range of fluid mechanical operating conditions compared to the work of Sharma et al. [40]. Of particular interest are conditions where impacting droplets *do not detach* from the air/bulk interface. As shown in the Section 3.2, this regime offers the possibility of creating thin fibers from inelastic materials that are remarkably smooth and stable. This approach is demonstrated by experiments creating highly oriented collagen fibers, which suggests that translating miscible jets are subject to large extensional deformations. In the case of collagen, these extensional stresses lead to strong alignment of fibrils that can be of great utility for a number of applications. For example, in tissue regeneration this orientation of collagen fibrils is able to provide contact guidance to mammalian cells, which is important for anisotropic tissues, such as nerve guides and vascular grafts.

The interaction of miscible fluids presents interesting challenges and important opportunities. This work can be roughly split into two parts: (1) the impaction of drops with a second, miscible bulk liquid with a particular focus on drops that are "pinned" by the air/bulk interface and then descend as "free-surface pendant" drops or "sagging blobs" within the second fluid and (2) the interaction of submerged miscible jets. The first part represents a focus into regions of the phase diagram of miscible drop morphologies reported recently by Sharma et al. [40] that has not been deeply explored. These processing conditions suggest possible ways to produce slender, well-oriented filaments from inelastic materials, and this advantage is considered in detail in the second part of the paper where we demonstrate that highly oriented fibers can be fashioned.

2 Experimental

2.1 Drop impact

Typical experiments investigating sedimenting, miscible drops have them ejected from a specified height above an air/bulk liquid interface. Depending on the kinetic energy of the droplet, a number of subsequent events are possible upon impact. The impact velocity, U_i, is set by the release height, which, in turn, sets the "impact" Reynolds number,

$$Re_i = \frac{\rho_b U_i D}{\eta_b}, \tag{2}$$

where ρ_b is the density of the bulk, D is the equivalent spherical diameter associated with the volume of the drop, and η_b is the bulk viscosity. This velocity also controls the "impact" Weber number,

$$We_i = \frac{\rho_d U_i^2 D}{\sigma_{ba}}, \tag{3}$$

where ρ_d is the drop density, and σ_{ba} is the interfacial tension between the bulk liquid and the air. During impact, a number of events can ensue, depending on the impact Reynolds number, the impact Weber number, the Froude number,

$$Fr = \frac{U_i}{\sqrt{Dg}}, \tag{4}$$

and the viscosity ratio, the density ratio, and the surface tension ratio

$$\beta_\eta = \frac{\eta_d}{\eta_b}; \quad \beta_\rho = \frac{\rho_d}{\rho_b}; \quad \beta_\sigma = \frac{\sigma_{da}}{\sigma_{ba}}, \tag{5}$$

where η_d and ρ_d are the droplet viscosity and density, respectively. Buckingham-Π theory states that this set of six dimensionless groups $\{Re_i, We_i, Fr, \beta_\eta, \beta_\rho, \beta_\sigma\}$ spans the parameter space of the available variables $\{D, U_i, g, \rho_b, \eta_b, \sigma_{ba}, \rho_d, \eta_d, \sigma_{da}\}$.

Previous work has primarily examined the case where impaction is sufficient to cause *detachment* of the droplet from the air/bulk interface. The shape evolution of the detached, sedimenting drops has then been the subject of investigation, and those shapes are largely affected by the "sedimentation" Weber number,

$$We_s = \frac{\rho_d U_s^2 D}{\sigma_{bd}}. \tag{6}$$

where U_s is the sedimentation velocity of the drop, and σ_{bd} is the interfacial tension between the miscible bulk and drop liquids. In most cases, previous work has left the value of the interfacial tension, σ_{bd}, *undetermined*, as the reliable measurement of the value is beyond current technologies.

In this work, we will focus on impact observations made in the parameter space consisting of the viscosity ratio and a value that we will call the drop Weber number,

$$We_d = \frac{We_i}{\beta_\sigma} = \frac{\rho_d U_i^2 D}{\sigma_{da}}, \tag{7}$$

which is simply the product of the impact Weber number and the inverse of the surface tension ratio.

Following Rein's survey of governing parameters, we will focus on spherical liquid drops impacting normally on a deep, flat liquid surface of a different material [33]. Since we are interested in the impaction of the droplets, we will assume that no internal circulation is present and that the drop is not deformed into an elliptical shape by aerodynamic forces, as the drops will be relatively viscous in nature. The presence of internal circulation (combined with drop oscillations) may be responsible for penetrating vortex rings [10], as well as contributing to bubble capture [18, 30, 32, 34]. A number of studies have been completed on the subject of bubble entrapment in various drop/bulk combinations [5, 11, 12]; however, the main focus has been on water droplets impacting a water bath [14, 25, 30–32]. Major efforts have been spent on understanding the effects of the thin film of air that can separate the drop from the bulk prior to impact [28, 35, 36]. Influenced by the rate at which the film thins, this cushion of air can prevent the instantaneous interfacial rupture that leads to coalescence.

Other studies have shown that the ambient gas can affect the impact outcome [38, 47, 49]. We are neglecting the influence of the gaseous state (air) outside of the surface tension with the bulk and with the drop, respectively.

2.1.1 Drop impact fluids

The fluids chosen for this study were water for the bulk and glycerol for the impacting miscible droplets. Water was chosen for the bulk to reduce costs as well as to allow the more viscous droplets to penetrate the bulk significantly, allowing formation of the varying morphologies. Glycerol is a common Newtonian fluid that readily diffuses into water. The properties of these glycerol-water solutions are easily tunable based on the concentration of glycerol in the mixture; however, care must be taken as glycerol is known to be hygrophilic, appreciably pulling water from the atmospheric air.

2.1.2 Physical properties

Physical properties of the two impacting drop test fluids can be found in Table 1. Glycerol is seen to be more viscous and more dense than the bulk water, while having lower surface tensions.

Table 1: Physical properties of drop impact test fluids.

Solution	β_ρ	β_η	β_σ
Water	1	1	1
Glycerol	1.264	1400	0.86

When pure glycerol is mixed with varying levels of water, a significant change in the physical properties of the ma-

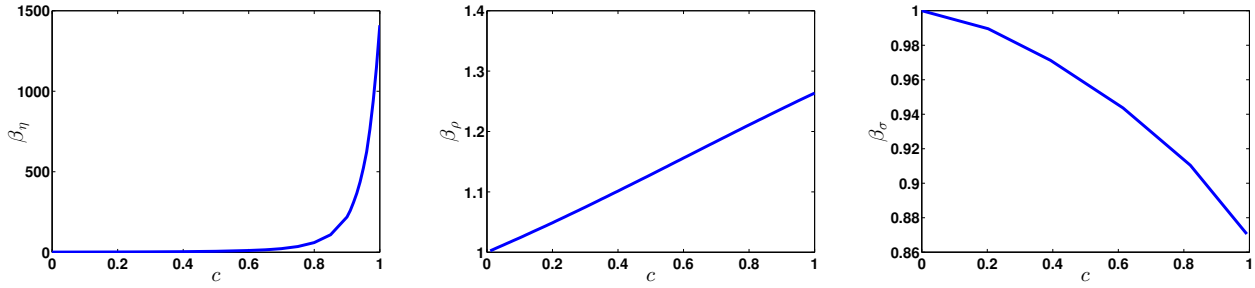

(a) $\beta_\eta$versus c (b) $\beta_\rho$versus c (c) $\beta_\sigma$versus c

Fig. 1: Glycerol properties. (a) Plot of viscosity ratio of glycerol as a function of concentration. The viscosity of the solution is very nonlinear, varying three orders of magnitude and decaying rapidly as the concentration of glycerol decreases. (b) Plot of specific gravity of glycerol as a function of concentration. (c)Plot of surface tension ratio of glycerol as a function of concentration. All data was reported at a temperature of 20°C relative to water [4].

terial will occur [4]. Specifically, the viscosity of the glycerol-water solution decays rapidly and very nonlinearly with increasing amounts of water before leveling below a certain concentration (see Figure 1(a)). Figure 1(b) also shows that the density of the solution will decay with increasing water content, but the decay is linear, and the percentage of change is much smaller. Likewise, the surface tension of the glycerol-water solution will change, increasing nonlinearly with increasing water content, but, again, the overall percentage of change is small (see Figure 1(c)). Since the range of the change in viscosity ratio of [1,1400] is significantly larger than the range of the change in density ratio of [1,1.264] or surface tension ratio of [0.86,1], understanding the effect of changes in the viscosity were initially investigated.

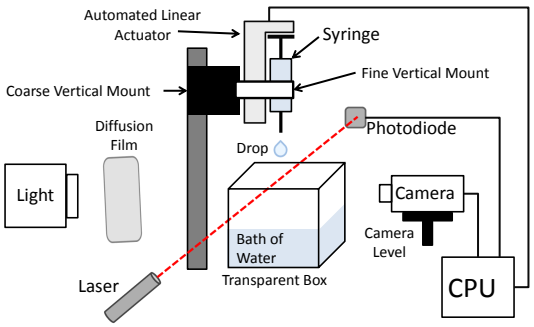

Fig. 2: Schematic of the drop impact setup. A computer controlled syringe ejects a droplet from a predetermined height. The droplet traverses a laser triggering mechanism, initiating the high-speed imaging, prior to impacting in the bulk water.

2.1.3 Drop impingement apparatus

An apparatus for drop impaction studies was built as shown in Figure 2. Experiments proceed by elevating a syringe to a specified height above a bulk liquid, which can be finely tuned using a micrometer. A computerized linear actuator is used to dispense a pendant drop from the syringe. Capillary breakup of the pendant drop releases the droplet from a 13-gauge, flat-tipped needle, and, once it traverses a laser triggering mechanism, a high speed camera (Photrom Fastcam MC2) captures its fate at a rate of either 3000 or 5000 frames per second. The drops are visible through strong gradients in their indices of refraction. We have conducted a range of experiments employing several drop/bulk liquid pairs including (glycerin-water)/(water), as reported in this work. Drops consisting of varying concentrations of glycerol-in-water were dropped into water that had been filtered using a Millipore Milli-Q A10. The glycerol was mixed with filtered water to the desired concentration. The physical properties of each glycerol solution were measured prior to each set of trials.

To characterize variations in the impact conditions for each experiment, the high-speed videos were analyzed using an in-house image processing routine written in MATLAB^{TM}. The routine uses an evolving domain scheme to track the droplet as it approaches the air/bulk surface. From the tracking, information about the drop diameter and the drop impact velocity can easily be calculated by referencing an item in the image with a known dimension. Further, any deformation of the falling droplet from the assumed spherical state can be observed to ensure that significant oscillations are not occurring prior to impact.

2.2 Fiber formation

2.2.1 Submerged jet apparatus

An apparatus for submerged fiber formation studies was built as shown in Figure 3. An exploded assembly of the apparatus, shown in Figure 3(a), shows two o-rings used to vacuum seal a particular substrate to the device. The inter-

changeability of the substrate provides flexibility in the orifice diameter. Experiments proceed by filling the transparent box with a bulk reagent. Then, the fiber material is pushed into the void between the base and the substrate before being expelled into the bulk system. A horizontal view of the apparatus in action visually shows the fiber being ejected through the orifice into the bulk (see Figure 3(b)).

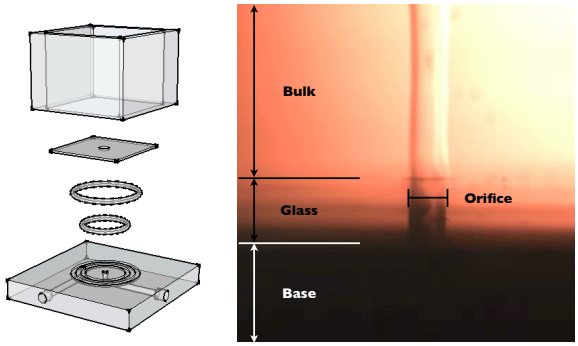

(a) Assembly (b) Collagen fiber

Fig. 3: Fiber formation apparatus. (a) Exploded assembly of the submerged jet setup. The base was created to allow for an interchangeable substrate to be vacuum sealed to the base with two o-rings creating a seal. Transparent walls were adhered to the base to allow for visualization from the side. (b) An upward jet of the collagen solution into PBS. The substrate is a piece of glass with an office diameter of 0.76 mm. The collagen goes through a sol-gel transition, forming a continuous fiber with a swollen diameter on the order of the orifice diameter.

The volumetric flow rate of the jet that was used when we created the collagen fiber was about 5.7 mm^3/s, and the fiber formation was halted after a total of 280 mm^3 of collagen solution was expelled.

2.2.2 Fiber materials

For the collagen fiber experiment, a stock solution of concentrated rat tail collagen type I (BD Biosciences) 9-10 mg/ml in 0.02 N acetic acid, pH 3.5, was used. The collagen was injected into a buffer of 10x phosphate-buffered saline (PBS) (Gibco-Invitrogen), pH 7.4, at 37°C, causing the collagen solution to undergo fibrillogenesis of the collagen molecules. The fiber became opaque as the collagen fibrils were formed.

2.2.3 SEM

For SEM imaging, the following standard SEM specimen preparation was used, where the fiber was treated with Karnovsky's fixative (4% paraformaldehyde/2.5% glutaraldehyde in 0.1 M sodium cacodylate, pH 7.3) (Electron Microscopy Sciences) while in storage.

Two separate techniques were used to treat the specimen prior to SEM imaging. The first technique was to simply place the specimen in a vacuum desiccator containing anhydrous calcium sulfate (Drierite) overnight.

The alternative technique was to first dehydrate the specimen through a gradient of ethanol (30%, 50%, 70%, 80%, 90%, 95%, and 99.5%) for 10 minutes each, rinsing twice with Milli-Q water in between. The specimen was then placed in a vacuum desiccator for two hours.

The two samples were then sputter coated with PdAu particles to create a layer thickness of 100 Å.

3 Results and Discussion

3.1 Glycerol drop/water bath impact morphologies

The impact of miscible glycerol-water solutions with a target bath of water can create a number of morphologies as represented by the samples provided in Figure 4. Example trials show a number of different characteristics that can be used to categorize the droplets into separate regimes. Figure 4(a) shows the well-known toroidal strand. In Figure 4(b), an axisymmetric lens is seen just below the air/bulk interface with a clean entrance through the interface. Affectionately referenced a jellyfish, Figure 4(c) shows a lens with a skirt being drug back towards the air/bulk interface and an entrained bubble on the drop/bulk interface. A very large entrained bubble detached from a lens-like morphology is seen in Figure 4(d). Figure 4(e) shows a very elaborate axisymmetric tiered morphology that can exist. Figure 4(f) shows a central jet that has not detached, but the initial droplet has been elongated up inside the jet. If the central jet were to detach, a second impact would result after the detached droplet returned to the surface. Figure 4(g) shows a residual halo that can form around a pinned drop that has impacted at relatively high We_d, following a central jet event, while Figure 4(h) shows the chaotic aftermath of a detached jet that has impacted the surface a second time. Prior to the second impact, a blob-like morphology resided on the interface.

To objectively map the various morphologies that exist, we chose three different criteria to examine, allowing us to distinguish different trials. In some cases, we attempted to make further distinctions beyond the initial criteria to create subsets inside of the two disjoint sets. First, we separate those trials that had the air/bulk interface rebound above the initial horizontal plane, which is a nice criterion for the onset of a central jet, often called a Worthington jet after Worthington's popularized work or a Rayleigh jet after the detachment of the end of the jet by capillary (or Rayleigh) breakup. Next, we distinguished those trials that caught a bubble from those trials that did not and mapped this transition with the appearance of the onset of a central jet to

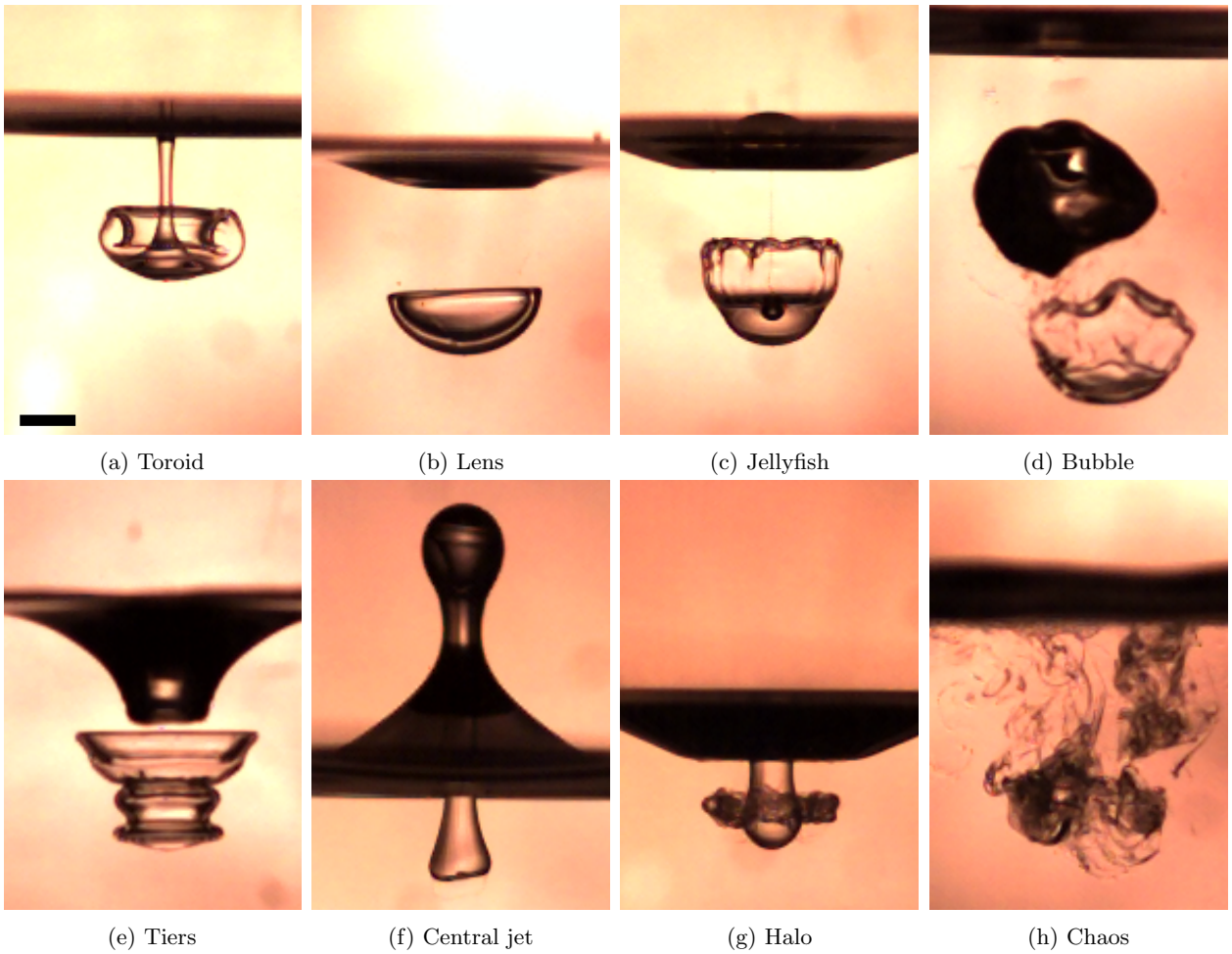

(a) Toroid (b) Lens (c) Jellyfish (d) Bubble

(e) Tiers (f) Central jet (g) Halo (h) Chaos

Fig. 4: Glycerol drop into water bath impact morphology examples. The projection of the air/bulk interface is seen as the large black area spanning each photograph. (a) A toroidal strand ($\beta_\eta = 71$, $We_D = 120$, $t = 0.049$s). (b) An axisymmetric lens ($\beta_\eta = 920$, $We_D = 480$, $t = 0.014$s). (c) A lens with an extending skirt and an entrained bubble on its interface ($\beta_\eta = 110$, $We_D = 190$, $t = 0.036$s). (d) A very large entrained bubble, detached above a lens-like morphology ($\beta_\eta = 1,200$, $We_D = 1,500$, $t = 0.057$s). (e) An axisymmetric tiered morphology ($\beta_\eta = 310$, $We_D = 580$, $t = 0.026$s). (f) A central jet that has not detached ($\beta_\eta = 71$, $We_D = 550$, $t = 0.071$s). Notice that the droplet has been elongated up inside of the jet. (g) A residual halo around a pinned drop after a central jet event ($\beta_\eta = 71$, $We_D = 290$, $t = 0.033$s). (h) The chaotic aftermath of a detached central jet that has impacted the surface a second time ($\beta_\eta = 163$, $We_D = 1400$, $t = 0.21$s). Length scale in (a) is 3 mm, which is consistent for all of the trials.

show a general correlation of momentum dissipation. Finally, we attempt to determine whether the majority of the droplet continues to be attached or pinned to the air/bulk interface versus those trials showing the drop pass "cleanly" through the air/bulk interface without any persisting tail.

The results shown in the following sections are for a miscible glycerol-water droplet impacting a water bath. To vary the viscosity ratio, the concentration of the glycerol-water solutions was varied. To vary the drop Weber number, the height of the syringe tip above the air/bulk interface is systematically varied over a range of one drop diameter to one meter. The range of drop diameters for these trials is $[4.6, 5.5]$ mm, and the range of velocities for these trials is $[0.16, 4.3]$ m/s. The same trials are shown for all three designations. The larger velocities are approaching the same order of magnitude as the terminal velocities that are predicted to be on the order of 10 m/s (terminal velocity of water with a diameter of 5 mm is approximately 9 m/s [13, 17]). Note that the terminal velocity scales with the density difference of the two fluids and the inverse of the outer media viscosity.

3.1.1 Central jet

The onset of a central jet for various drop/bulk combinations has been previously studied; however, recent studies have not focused on a miscible two-fluid system of varying viscosity ratios. The results shown in Figure 5 show a phase diagram of a central jet, seen when the air/bulk interface deflects above the initial horizontal interface. Further designa-

tion is made for the central jet as to whether the jet detached before returning to the surface or not. In general, the plots show the presence of a central jet occurring at higher drop Weber numbers and lower viscosity ratios, while detached central jets occur at even higher drop Weber numbers than the regular central jets.

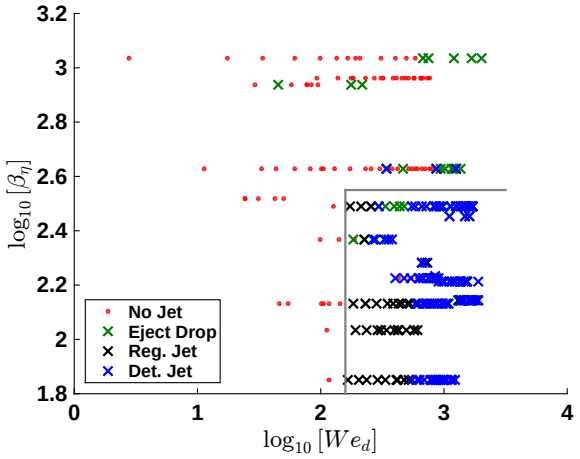

Fig. 5: Phase diagram of central jet morphologies as a function of viscosity ratio and drop Weber number. The presence of a central jet consistently occurs at higher drop Weber numbers and at lower viscosity ratios. The presence of a detached central jet (Det. Jet) over a regular jet (Reg. Jet) correlates with a continued increase in drop Weber number. The presence of an ejected droplet appears to be randomly dispersed throughout the trials.

Also shown in Figure 5 are trials where a droplet, at least an order of magnitude smaller in diameter than the initial impacting droplet diameter, D, was ejected from the bulk. These trials, where a standard central jet was not seen, are thus denoted as an ejected droplet. Interestingly, crowning droplets, where the outer rim of the splash begins to detach, are often reported in these types of droplet impaction studies, but we did not view any such droplets under the conditions that we sampled.

Literature has discussed this presence of a central jet as the transition from coalescence to splashing in a homogeneous system. Hsiao et al. described the Weber number as a ratio of time scales of surface tension (τ_σ) to convection (τ_U), stating that, for a homogeneous system, when the convection time scale becomes much smaller than the surface tension time scale, a splashing event will occur [19].

$$We_d = \left[\frac{\tau_\sigma}{\tau_U}\right]^2 \quad \ni \quad \tau_\sigma = \sqrt{\frac{\rho_d D^3}{\sigma_{da}}}; \quad \tau_U = \frac{D}{U_i}. \tag{8}$$

Further, Thomson and Newall stated that, for a homogenous system, a low viscosity ratio will result in splashing while an increase in viscosity ratio will lead to coalescence [43]. Thus, the critical impact Weber number must be dependent on the viscosity ratio, and we have seen a similar dependence for both parameters in the two-fluid system.

3.1.2 Bubble capture

Air entrainment during drop impaction has been studied extensively for homogeneous drop/bulk systems; however, very few studies have been interested in different fluids and even less in a miscible two-fluid system. The results shown in Figure 6 show the same trials seen in Section 3.1.1 on the presence of a central jet; however, the phase diagram now also distinguishes between the presence of bubble capture morphologies as a function of viscosity ratio and drop Weber number. The capturing of bubbles was then split into two subcategories depending on how the bubble was initially captured immediately after passing through the air-water interface – note that all of the bubbles will eventually be detached or released from the interface, since the fluids are miscible. If the bubbles reside at the interface of the drop and the bulk, they are designated as being interfacial bubbles (see Figure 4(c) for an example). Alternatively, if the bubbles are detached from the interface into the bulk fluid, they are designated detached bubbles (see Figure 4(d) for an example). A third option can exist where the bubble is detached from the interface into the drop medium. Although we have seen this phenomena regularly for other drop/bulk combinations such as heavy immiscible oils dropping into water, we viewed only two such trials having this phenomena for the glycerol-water drop and water bath system under the conditions that we viewed.

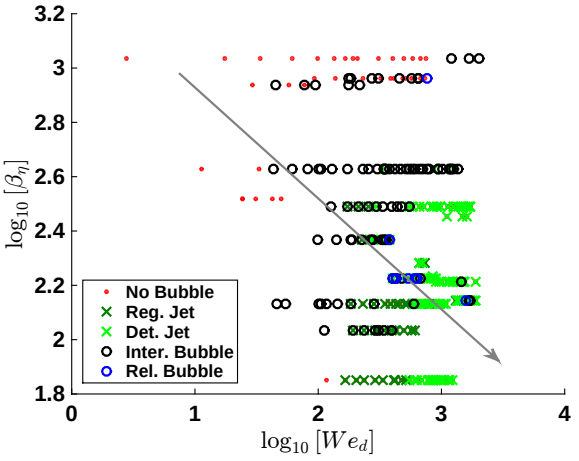

Fig. 6: Phase diagram of bubble capture and central jet morphologies as a function of viscosity ratio and drop Weber number. Bubble capture can be split into bubbles that reside at the interface of the drop and the bulk (Inter. Bubble) and bubbles that are released from the interface (Rel. Bubble). A general transition from no bubbles to bubbles to central jets can be seen from upper left (high β_η and low We_d) to lower right (low β_η and high We_d).

In viewing Figure 6, the capturing of bubbles appears to exist at a variety of viscosity ratios. A correlation with the drop Weber number appears to exist where bubbles that are caught at the drop/bulk interface tend to have a lower drop Weber number than those bubbles that are released from the interface. The order of bubble entrainment and no bubble entrainment seems to depend on factors beyond the two metrics used; however, in general, regions of groupings between the disjoint sets do seem to exist. These factors may include physics concerning the internal circulation of the droplet, drop oscillations, and bubble entrapment during initial impingement. To better explain these groupings, the bubble onset has been plotted in Figure 6 on top of the presence of a central jet. This relations shows that a general sweeping trend exits from high viscosity ratio and low drop Weber number to low viscosity ratio and high drop Weber number. Along this trend, the morphologies transition from no bubbles or central jets to bubbles to central jets to detached central jets.

At this point, we can describe this correlation in terms of forces. In one limit, no bubbles are encapsulated when the viscosity ratio is high and the drop Weber number is low. Under these conditions, the inertia needed to deflect the air/bulk interface is low, and the surface tension of the drop is high, opposing any drop deformations. Further, increased viscosity restricts any flow of the drop. In the other limit, a central jet is formed when the viscosity ratio is low and the drop Weber number is high. Thus, the inertia needed to deflect the air/bulk interface is high enough, but the surface deflects too much, creating a large upward motion before any bubbles are encapsulated. In between these two limits exists a region where the viscosity ratio is low enough to allow flow and enough inertia exists to deflect the air/bulk interface substantially but not too much. Here, the deflection closes on itself, encapsulating a bubble in the process.

A few trials were seen where multiple bubbles were entrained. Among this small subset, trials did exist where one of the bubbles was detached while another bubble was caught. The size of the bubbles also varied widely; however, bubbles having diameters on the order of the initial drop diameter, D, similar to the bubble seen in Figure 4(d), were often released into the bulk. Bubbles having diameters much smaller than D, similar to the bubble seen in Figure 4(c), often remained attached to the drop/bulk interface.

3.1.3 Breakthrough versus strand

A major aim of this study was to identify appropriate conditions where the sagging blob or pinned free-surface pendant drop phenomena was present. Figure 7 uses the same trials as seen in Sections 3.1.1 and 3.1.2 to distinguish between the presence of a pinned tail of the drop to the air/bulk interface and a clean entrance into the bulk, denoted as breakthrough. The pinned trials are further distinguished into subsets where the presence of a sagging blob (see Figure 8) is separated from the toroidal strand morphologies seen similar to Figure 4(a). To distinguish the difference, we denote sagging blobs as occurring when the momentum of the droplet has been completely suppressed (momentumless coalescence [2]), creating a situation where the velocity of the leading edge of the droplet is negligible relative to the timescale of the experiment. Other pinned trials exist where the droplet continues to move down with a tail attached to the air/bulk interface trailing the droplet.

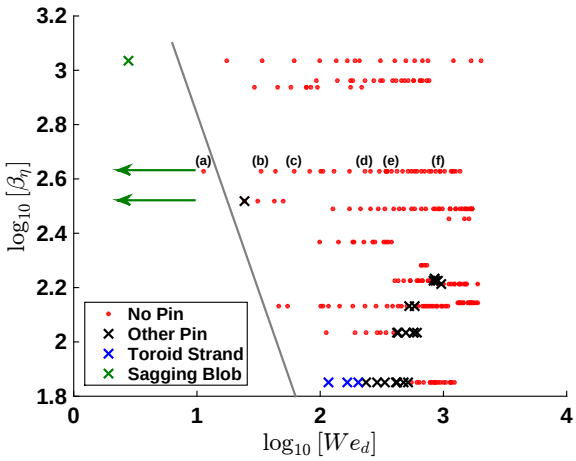

Fig. 7: Phase diagram of pinned morphologies as a function of viscosity ratio and drop Weber number. Impact velocities of pinned drops are often difficult to measure, as drops may bridge between the syringe and the bulk prior to releasing from the syringe. Green arrows show where these trials would exist with their correspondingly small drop Weber number as seen in Figure 8. Pinned trials can be of sagging blobs, toroidal strands, or others such as halos following a central jet. The data points (a)-(f) correspond to Figures 11(a)-(f) respectively.

Since the presence of the sagging blob is quite difficult to achieve for some drop/bulk combinations, the syringe often becomes too close to the air/bulk interface for the droplet to completely detach from the syringe prior to impacting the air/bulk interface, and the drop essentially bridges the gap. Thus, the drop Weber number, which is a function of the impact velocity, no longer has a measurable quantity. However, the value of the impact velocity and the resulting inertial effects are obviously being reduced by the continued interaction with the syringe, so the drop Weber number is being effectively reduced. Situations where a sagging blob is created by a bridged droplet are depicted qualitatively by the arrows, where, for the parameters being used, the sagging blob morphology occurred for all drop Weber numbers below a certain value. In this regime, the trials as exemplified in Figure 8 were easily reproducible. Not shown on this graph exists a lower limit in the viscosity ratio around $\log_{10}[\beta_\eta] \approx 2.4$. Below this viscosity ratio, the drop will spread, wetting the

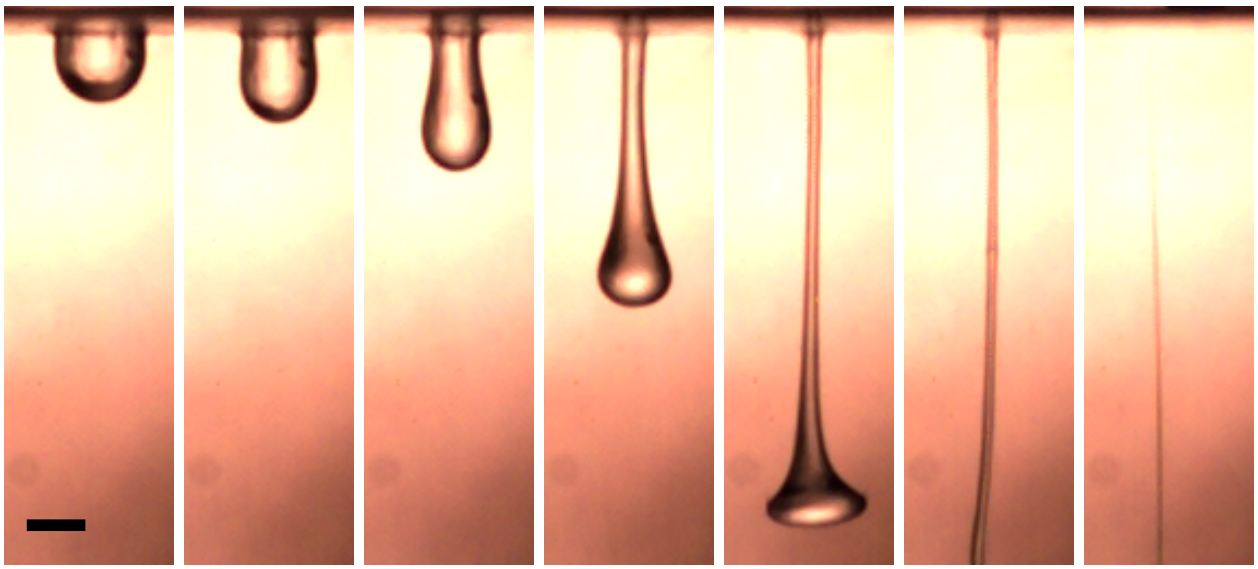

(a) 0.0s (b) 0.1s (c) 0.2s (d) 0.3s (e) 0.4s (f) 0.5s (g) 1.5s

Fig. 8: The formation and evolution of a sagging blob descending to pull a slender filament ($\beta_\rho = 1.243$, $\beta_\eta = 330$). Length scale in (a) is 3 mm, which is consistent for all of the trials. Time scale is relative to (a).

interface and creating a film at the air/bulk interface. If the viscosity ratio is high enough, the wetting of the interface is resisted, and the majority of the drop material will remain in a blob; however, some wetting still occurs, and this film contributes to the extended pinning to the interface.

The sequence of photographs in Figure 8 shows the evolution of a blob that was "pinned" by capillary forces at the interface. As time proceeds, the drop/bulk interfacial tension decreases with time, and the blob sags under gravity, pulling a slender filament behind it. Remarkably, this filament does not break and continues to stretch as it is fed by the descending droplet. This process of creating slender filaments from inelastic liquids is the focus of the application presented in the Section 3.2 using collagen as an example.

A complex sequence of events leading to the formation of sagging, miscible blobs exists. Not shown in Figure 8 are the first stages of impact where drops in this region of the phase diagram flatten upon impact and spread radially across the air/bulk interface. Upon cessation of the spreading, gravitational forces draw the reservoir of heavier, drop liquid into a sagging blob, such as the one shown at $t = 0.1s$ in Figure 8.

Alternatively, Figures 9 and 10 show the impact sequence of two trials that break through the interface. Drops that cleanly break through the interface go through a common transition away from the pinned sagging blob to the central jet. Figure 11 shows how this transition begins at low drop Weber numbers with (a) tear drop shapes, (b) ellipsoidal drops, and (c) disc-like shapes, before forming (d) symmetric lens, (e) jellyfish, and finally (f) tiers at higher drop Weber numbers. Figure 9 corresponds with the impact sequence that resulted in the ellipsoidal drop seen in Figure 11(b). Figure 10 corresponds with the impact sequence that resulted in the tiered drop seen in Figure 11(f).

3.2 Collagen fiber formation

By operating an extruder in a region of constant, low jet Weber number (We_j) and high viscosity ratio $\left(\beta_\eta = \frac{\eta_j}{\eta_b}\right)$, reminiscent to the drops that produce the stable filaments as shown in Figure 8, we are able to continuously draw filaments of materials that otherwise lack the elasticity necessary to use conventional spinning operations. The low jet Weber number is analogous to the sedimentation Weber number,

$$We_j = \frac{\rho_j U_j^2 h}{\sigma_{bd}}, \tag{9}$$

where ρ_j, U_j, and h denote the jet density, velocity, and radius, respectively. Thus, the low initial interfacial tension forces between the jet and the bulk prevents droplet breakup, while the low inertial forces, caused by the low jet velocity similar to the momentum-less coalescence seen in the sagging-blob regime, prevents the jet from having non-linear modes of breakup (i.e., low jet Reynolds numbers). The constant flow allows the fiber to be continuously created, as gravity is pulling the fiber vertically. Thus, a balance is created between high viscous forces, low interfacial tension

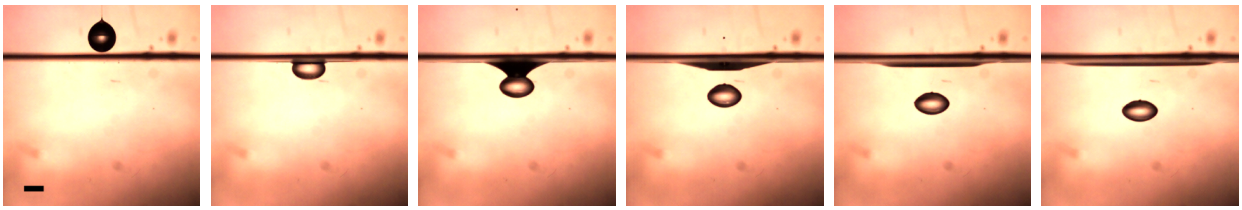

(a) 0.00s (b) 0.01s (c) 0.02s (d) 0.03s (e) 0.04s (f) 0.05s

Fig. 9: Impact sequence of breakthrough for the ellipsoidal drop example of glycerol-water solutions into water ($\beta_\eta = 410, We_D = 33$) seen in Figure 11(b). Length scale in (a) is 3 mm, which is consistent for all of the trials.

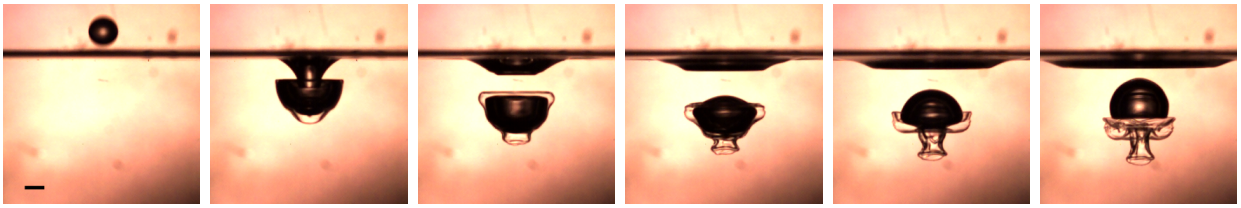

(a) 0.00s (b) 0.01s (c) 0.02s (d) 0.03s (e) 0.04s (f) 0.05s

Fig. 10: Impact sequence of breakthrough for the tiered drop example of glycerol-water solutions into water ($\beta_\eta = 410, We_D = 940$) seen in Figure 11(f). Length scale in (a) is 3 mm, which is consistent for all of the trials.

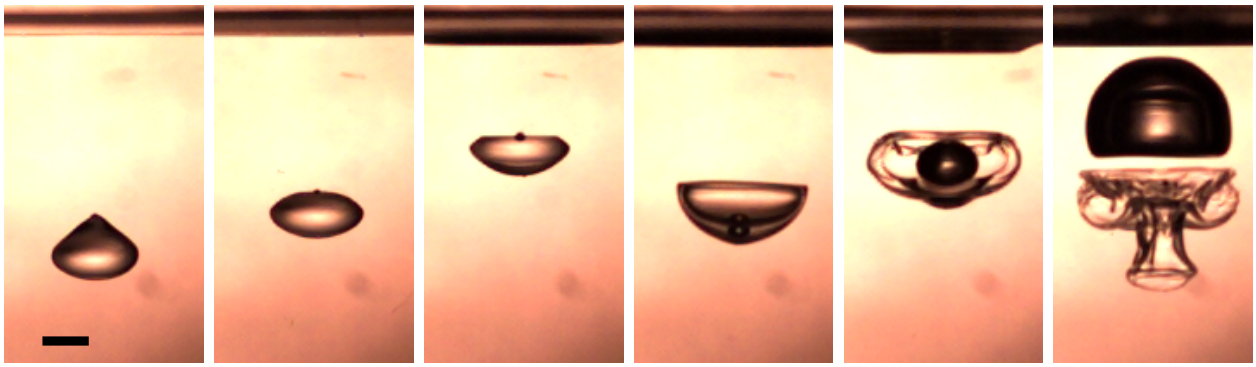

(a) Tear (b) Ellipse (c) Disc (d) Lens (e) Jellyfish (f) Tiers

Fig. 11: Breakthrough examples of glycerol-water solutions into water ($\beta_\eta = 410$). At low drop Weber numbers (a) tear drop shapes ($We_D = 11$, $t = 0.15$s), (b) ellipsoidal drops ($We_D = 33$, $t = 0.088$s), and (c) disc-like shapes form ($We_D = 62$, $t = 0.034$s). At higher drop Weber numbers (d) symmetric lens ($We_D = 230$, $t = 0.038$s), (e) jellyfish ($We_D = 380$, $t = 0.028$s), and finally (f) tiers ($We_D = 940$, $t = 0.055$s) exist. Length scale in (a) is 3 mm, which is consistent for all of the trials. Time scale is relative to initial impact.

forces, and low inertial forces (i.e., high viscosity ratio, low Reynolds number, and low Weber number), leading to a high capillary number (ratio of viscous to capillary forces) that slow and suppress the Rayleigh instability (capillary breakup) of these Newtonian jets. Once a desired filament is drawn, "freezing" this morphology in place through either a chemical reaction or a physical phase transition is necessary. For the purpose of demonstrating this concept, we have chosen the sol-gel process undertaken by collagen protein. In the case of collagen, these extensional stresses lead to strong alignment of fibrils that can be useful for numerous applications.

Collagen is a triple helix of polypeptide chains and is the most prevalent protein in the human body. This rodlike structure is used in load bearing tissue, and it is a major component of the extracellular matrix. Most prevalently, it is found in the form of fibers formed from self-assembly of these rods. However, collagen does form a molecular solution with an absence of fibers when dissolved at low pH in solvents such as acetic acid. In solution and at high concentration, collagen rods are remarkably easy to orient by

relatively weak hydrodynamic forces [22, 24]. Introduction of collagen-acetic acid solutions to neutral pH buffer solutions will induce a sol-gel transition, and the material will rapidly form a gelled network of collagen microfibers. This fibrillogenesis reaction is rapid, but it can be controlled by adjusting sodium phosphate and collagen concentrations. In the context of the use of miscible, multiphase flow to generate slender fibers of collagen, we have expelled streams of collagen solution into 10x phosphate-buffered saline (PBS) solution at 37°C. The protein solution was rat tail collagen type I at 9-10 mg/ml in 0.02 N acetic acid, pH 3.5.

Because the collagen solutions are less dense than the PBS solutions, the pendent drops were initiated in an *inverted* orientation, and the injection of collagen was upward into the media. The fiber produced is shown in Figure 12 to be very uniform in diameter and on the order of 65 μm in diameter, making the swollen diameter of the fiber on the order of the orifice diameter. The photographs also demonstrate the ability of the miscible multiphase flow injection scheme to produce highly oriented and uniform fibers. This process is particularly interesting in the case of collagen, since these solutions are inelastic and difficult to process into fibers with spinning operations. Highly oriented collagen has important advantages when fibers are used in medical applications. In particular, the highly oriented collagen fibrils induce "cell guidance" for cells growing on their surface. This guided growth is shown in Figure 4(a) of Lai et al. [24], where they present an SEM image of a single fibroblast cell that is attached to the collagen fibril surface and elongated along the fibril longitudinal axis. The ability to guide the orientation and migration of cells is critical to the regeneration of anisotropic tissue such as blood vessels, nerve guides, and lymphatic tubes. The image in Figure 12 reveals that the collagen fibrils produced in this fashion are remarkably well oriented along the main fiber axis, and evidently, the flow of this miscible jet produces large, elongational deformations that are reminiscent of "filament stretching extensional flow" (FISER) processes [27].

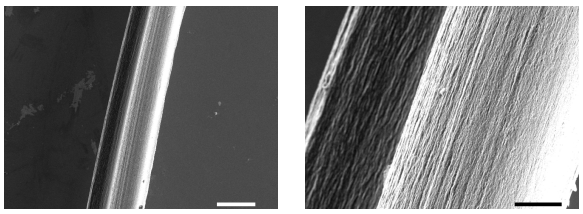

(a) SEM (b) SEM

Fig. 12: Collagen fiber formation from a jet of miscible collagen/acetic acid solution issuing into a neutral PBS solution. (a) SEM picture of the resulting, gelled fiber with a diameter of approximately 65 μm. Length scale is 50 μm. (b) Close-up of the fiber showing highly oriented collagen fibrils along the jet direction. Length scale is 10 μm.

4 Conclusions

The vast majority of previous work on miscible drop impact has explored regimes where isolated, descending drops are presented to a bulk medium. The resulting intricate drop shapes that evolve as a result of a small and diminishing interfacial tension are then recorded. As mentioned above, Sharma et al. were able to construct a phase diagram in the parameters of the viscosity ratio and the impact Reynolds number that depicts transitions in drop shapes as these dimensionless groups are varied. This work expands the parameter space by also considering strong changes in the Weber number, which ultimately leads to fiber formation.

Of particular interest are impaction measurements at *higher viscosity ratios* – at least an order of magnitude higher than the values reported by Sharma et al. [40]. In this regime, a phase transition between drops that "break through" the air/bulk interface and those drops that are "pinned" by the interface is uncovered. The phase boundaries reported by Sharma et al. identified different drop morphologies, and they were particularly interested in the "toroidal-spiral" (T-S) morphology similar to Figure 4(a); however, the viscosity ratio used in that work ranged from $2 \leq \beta_\eta \leq 14$, and the impact Weber number was in the range of $0.36 \leq We_i \leq 4.41$.

The phase boundary that we have uncovered is revealed at much higher viscosity ratios (on the order of $\log_{10}[\beta_\eta] \geq 2$), while still being at a relatively low impact Weber number (on the order of $We_i \leq 1$). As shown in the Section 3.2, drops formed in this We_i regime have the possibility of being "pinned" by the bulk interface and subsequently *stretching* into a filament while pinned to the surface. Additional morphological and dynamical transitions exist in the miscible drop impaction problem, and this work has explored a few of those transitions.

5 Acknowledgments

GGF acknowledges the grant NSF CBET 1335632 for partial support of this work. We would like to thank Ranulfo Allen and Edwina Lai for helping with the SEM imaging. We would like to thank Professor Eric S.G. Shaqfeh, Professor Patrick Anderson at Eindhoven University of Technology, Theresa Hsu, Armen Mekhdjian, and Saad Bhamla for useful discussions. We would also like to thank Nicholas Farn for his help during the summer of 2012.

References

1. Adachi, K., Kiriyama, S., Yoshioka, N.: The behavior of a swarm of particles moving in a viscous fluid. Chem Eng Sci **33**, 115 (1978)
2. Anilkumar, A.V., Lee, C.P., Wang, T.G.: Surface-tension-induced mixing following coalescence of initially stationary drops. Physics of Fluids A **3**(11), 2587–2591 (1991)

3. Arecchi, F.T., Buah-Bassuah, P., Francini, F., Pé rez-Garcia, C., Querciolif, F.: An experimental investigation of the break-up of a liquid drop falling in a miscible fluid. Europhys Lett **9**, 333 (1989)
4. Association, G.P.: Physical Properties of Glycerine and Its Solutions. Glycerine Producers' Association (1963). URL http://books.google.com/books?id=XpeaGQAACAAJ
5. Baumann, N., Joseph, D.D., Mohr, P., Renardy, Y.: Vortex rings of one fluid in another in free fall. Physics of Fluids A: Fluid Dynamics **4**(3), 567–580 (1992)
6. Bisighini, A., Cossali, G.E.: High-speed visualization of interface phenomena: single and double drop impacts onto a deep liquid layer. Journal of Visualization **14**(2), 103–110 (2011)
7. Bisighini, A., Cossali, G.E., Tropea, C., Roisman, I.: Crater evolution after the impact of a drop onto a semi-infinite liquid target. Physical Review E **82**(3), 036,319 (2010)
8. Cahn, J.W., Hilliard, J.E.: Free energy of a nonuniform system i interfacial free energy. The Journal of Chemical Physics **28**(2), 258 (1958)
9. Cai, Y.K.: Phenomena of a liquid drop falling to a liquid surface. Exp. Fluids **7**, 388–394 (1989)
10. Chapman, D.S., Critchlow, P.: Formation of vortex rings from falling drops. Journal of Fluid Mechanics **29**(01), 177–185 (1967)
11. Deng, Q., Anilkumar, A.V., Wang, T.G.: The role of viscosity and surface tension in bubble entrapment during drop impact onto a deep liquid pool. Journal of Fluid Mechanics **578**, 119–138 (2007)
12. Deng, Q., Anilkumar, A.V., Wang, T.G.: The phenomenon of bubble entrapment during capsule formation. Journal of Colloid and Interface Science **333**(2), 523–532 (2009)
13. Dingle, N., Lee, Y.: Terminal fallspeeds of raindrops. Journal of Applied Meteorology **11**(5), 877–879 (1972)
14. Elmore, P., Chahine, G., Oguz, H.: Cavity and flow measurements of reproducible bubble entrainment following drop impacts. Experiments in fluids **31**(6), 664–673 (2001)
15. Fujimatsu, T., Fujita, H., Hirota, M., Okada, O.: Interfacial deformation between an impacting water drop and a silicone–oil surface. Journal of Colloid and Interface Science **264**(1), 212–220 (2003)
16. Garcimartín, A., Mancini, H.L., Pérez-García, C.: 2d Dynamics of a Drop Falling in a Miscible Fluid. Europhysics Letters **19**(3), 171–176 (1992)
17. Gunn, R., Kinzer, G.D.: The terminal velocity of fall for water droplets in stagnant air. Journal of Meteorology **6**(4), 243–248 (1949)
18. Hasan, O., Prosperetti, A.: Bubble entrainment by the impact of drops on liquid surfaces. J. Fluid Mech **1219**, 143 (1990)
19. Hsiao, M., Lichter, S., Quintero, L.G.: The critical weber number for vortex and jet formation for drops impinging on a liquid pool. Physics of Fluids **31**(12), 3560–3562 (1988)
20. Hu, Y., Wang, Q., Wang, J., Zhu, J., Wang, H., Yang, Y.: Shape controllable microgel particles prepared by microfluidic combining external ionic crosslinking. Biomicrofluidics **6**(2), 026,502 (2012)
21. Joseph, D.D., Renardy, Y.Y.: Fundamentals of Two-Fluid Dynamics; Part II: Lubricated Transported, Drops and Miscible Liquids. Springer-Verlag, New York (1993)
22. Kirkwood, J., Fuller, G.G.: Liquid crystalline collagen: A self-assembled morphology for the orientation of mammalian cells. Langmuir **25**, 3200 (2009)
23. Kojima, M., Hinch, E., Acrivos, A.: The formation and expansion of a toroidal drop moving in a viscous fluid. Physics of Fluids **27**, 19 (1984)
24. Lai, E.S., Anderson, C.M., Fuller, G.G.: Acta Biomaterialia. Acta Biomaterialia **7**(6), 2448–2456 (2011)
25. Leng, L.J.: Splash formation by spherical drops. Journal of Fluid Mechanics **427**, 73–105 (2001)
26. Machu, G., Meile, W., Nitsche, L.C., Schaflinger, U.: Coalescence, torus formation and breakup of sedimenting drops: experiments and computer simulations. Journal of Fluid Mechanics **447**, 299–336 (2001)
27. McKinley, G.H., Sridhar, T.: Filament-stretching rheometry of complex fluids. Annu Rev Fluid Mech **34**, 375–415 (2002)
28. Peck, B., Sigurdson, L.: The three–dimensional vortex structure of an impacting water drop. Physics of Fluids **6**(2), 564–576 (1994)
29. Powell, R., Mason, S.: Dispersion by laminar flow. AIChE Journal **28**, 286 (1982)
30. Prosperetti, A., Oğuz, H.N.: The impact of drops on liquid surfaces and the underwater noise of rain. Annu. Rev. Fluid Mech **25**, 577–602 (1993)
31. Pumphrey, H.C., Crum, L.: Free oscillations of near-surface bubbles as a source of the underwater noise of rain. The Journal of the Acoustical Society of America **87**(1), 142–148 (1990)
32. Pumphrey, H.C., Elmore, P.A.: The entrainment of bubbles by drop impacts. Journal of Fluid Mechanics **220**, 539–567 (1990)
33. Rein, M.: Phenomena of Liquid-Drop Impact on Solid and Liquid Surfaces. Fluid Dynamics Research **12**(2), 61–93 (1993)
34. Rein, M.: The transitional regime between coalescing and splashing drops. Journal of Fluid Mechanics **306**, 145–165 (1996)
35. Rodriguez, F., Mesler, R.: Some drops don't splash. J. Coll. Inter. Sci **106**(2), 347–352 (1985)
36. Rodriguez, F., Mesler, R.: The penetration of drop–formed vortex rings into pools of liquids. J. Coll. Inter. Sci **121**(1), 121–129 (1988)
37. Schaflinger, U., Machu, G.: Interfacial phenomena in suspensions. Chem Eng Technol **22**, 617 (1999)
38. Schotland, R.: Experimental results relating to the coalescence of water drops with water surfaces. Discuss. Faraday Soc. **30**, 72–77 (1960)
39. Shankar, P.N., Kumar, M.: Vortex rings generated by drops just coalescing with a pool. Physics of Fluids **7**(4), 737–746 (1995)
40. Sharma, V., Szymusiak, M., Shen, H., Nitsche, L.C., Liu, Y.: Formation of polymeric toroidal-spiral particles. Langmuir **28**(1), 729–735 (2012)
41. Szymusiak, M., Sharma, V., Nitsche, L.C., Liu, Y.: Interaction of sedimenting drops in a miscible solution – formation of heterogeneous toroidal-spiral particles. Soft Matter **8**(29), 7556 (2012)
42. Taylor, G.I.: Film notes for low-reynolds-number flows. National Committee for Fluid Mechanics Films **21617** (1967)
43. Thomson, J.J., Newall, H.F.: On the formation of vortex rings by drops falling into liquids, and some allied phenomena. Proceedings of the Royal Society of London pp. 417–436 (1885)
44. Tomlinson, C.: On a new variety of the cohesion-figures of liquids. Phil. Mag. Ser **4**(27), 425–432 (1864)
45. Walker, T.W., Hsu, T.T., Frank, C.W., Fuller, G.G.: Role of shear-thinning on the dynamics of rinsing flow by an impinging jet. Physics of Fluids **24**(9), 093,102 (2012)
46. Wang, X.S., Zhao, X.D., Zhang, Y., Cai, X., Gu, R., Xu, H.L.: Experimental study on the interaction of a water drop impacting on hot liquid surfaces. Journal of Fire Sciences **27**(6), 545–559 (2009)
47. Willis, K., Orme, M.: Binary droplet collisions in a vacuum environment: an experimental investigation of the role of viscosity. Experiments in fluids **34**(1), 28–41 (2003)
48. Worthington, A.M.: A Study of Splashes. Longmans, Green, And Co, London (1908)
49. Xu, L., Zhang, W.W., Nagel, S.R.: Drop splashing on a dry smooth surface. Physical review letters **94**(18), 184,505 (2005)
50. Zhao, H., Brunsvold, A., Munkejord, S.T.: Investigation of droplets impinging on a deep pool: transition from coalescence to jetting. Experiments in Fluids **50**(3), 621–635 (2011)